

Fluidic Flow Assisted Deterministic Folding of Van der Waals Materials

Huan Zhao, Beibei Wang, Fanxin Liu, Xiaodong Yan, Haozhe Wang, Wei Sun Leong, Mark J. Stevens, Priya Vashishta, Aiichiro Nakano, Jing Kong, Rajiv Kalia,* and Han Wang*

Origami offers a distinct approach for designing and engineering new material structures and properties. The folding and stacking of atomically thin van der Waals (vdW) materials, for example, can lead to intriguing new physical properties including bandgap tuning, Van Hove singularity, and superconductivity. On the other hand, achieving well-controlled folding of vdW materials with high spatial precision has been extremely challenging and difficult to scale toward large areas. Here, a deterministic technique is reported to fold vdW materials at a defined position and direction using microfluidic forces. Electron beam lithography (EBL) is utilized to define the folding area, which allows precise control of the folding geometry, direction, and position beyond 100 nm resolution. Using this technique, single-atomic-layer vdW materials or their heterostructures can be folded without the need for any external supporting layers in the final folded structure. In addition, arrays of patterns can be folded across a large area using this technique and electronic devices that can reconfigure device functionalities through folding are also demonstrated. Such scalable formation of folded vdW material structures with high precision can lead to the creation of new atomic-scale materials and superlattices as well as opening the door to realizing foldable and reconfigurable electronics.

1. Introduction

Graphene and other atomically-thin Van der Waals materials have demonstrated exceptional mechanical properties^[1–3] such as high flexibility, low bending stiffness, and superior layer strength. Leveraged by these unique properties, two-dimensional (2D) materials can be folded into various super-lattice structures, giving rise to exotic physical properties emerged from the folded edge, the interface, the layer misalignment, and interlayer misorientation. Recently twisted bilayer graphene (tBLG) with a carefully designed twist angle has shown intriguing electronic properties such as Mott insulator transition,^[4,5] Van Hove singularity,^[6–9] and superconductivity,^[10–12] providing a powerful avenue towards exploring Moiré physics and twistronics.^[13] As these properties are dictated by precise tuning of the interlayer misorientations, a simple, clean technique that can create twisted 2D materials with high controllability and scalability is highly desirable.

In previous literature, tBLG can be obtained by consecutively transferring two graphene monolayers synthesized by chemical vapor deposition (CVD).^[14–17] However, it is difficult to control the twist angle of CVD graphene flakes, since it is hard to know the crystal orientation of each layer without sophisticated characterization tools such as transmission electron microscopes (TEMs).^[18] In addition, even if the crystal orientation of two graphene monolayer is well identified, it is still challenging to align them with a precisely controlled rotational angle. Other approaches to prepare tBLG such as direct CVD synthesis^[19] and “tear and stack” method,^[4,10] offer either limited controllability of the twist angle or poor scalability.

2. Results and Discussion

2.1. An Introduction to a Deterministic 2D Material Molding Technique

Here we report a universal technique for folding 2D materials at a predefined position and direction using micro-fluidic forces. This technique can easily prepare highly controllable tBLG and other twisted 2D materials without manually aligning


Dr. H. Zhao, X. Yan, Prof. H. Wang
Ming Hsieh Department of Electrical Engineering
University of Southern California
Los Angeles, CA 90089, USA
E-mail: han.wang.4@usc.edu

B. Wang, Prof. P. Vashishta, Prof. A. Nakano, Prof. R. Kalia
Collaboratory for Advanced Computing and Simulations
University of Southern California
Los Angeles, CA 90089, USA
E-mail: rkalia@usc.edu

Prof. F. Liu
Department of Applied Physics
Zhejiang University of Technology
Hangzhou 310023, P. R. China

H. Wang, Dr. W. S. Leong, Prof. J. Kong
Department of Electrical Engineering and Computer Sciences
Massachusetts Institute of Technology
Cambridge, MA 02139, USA

Dr. M. J. Stevens
Center for Integrated Nanotechnologies
Sandia National Laboratories
Albuquerque, NM 87185, USA

 The ORCID identification number(s) for the author(s) of this article can be found under <https://doi.org/10.1002/adfm.201908691>.

DOI: 10.1002/adfm.201908691

and stacking the flakes, nor identifying the crystal orientation. Using this method, both micrometer-scale exfoliated 2D material flakes and wafer-scale CVD-grown 2D material arrays can be folded in seconds, with sub-micrometer spatial accuracy. **Figure 1a** illustrates the folding process, which starts with spin-coating 3 wt% polyvinyl alcohol (PVA) solution onto a 90 nm SiO₂/Si wafer followed by 2 min baking at 90 °C to form a uniform PVA layer, typically with a thickness of ≈40 nm. Then 2D material sheets are transferred onto the PVA layer. PVA is naturally water-soluble,^[20] typically a 40 nm PVA film can be dissolved in warm water within a few seconds. However, high dose electron beam (EB) irradiation can crosslink the PVA molecules due to a thermal induced autoignition process.^[21] Therefore, the exposed PVA areas become insoluble in water, in this case PVA functions as a negative resist.^[22,23] To fold a 2D material sheet, the electron beam lithography (EBL) irradiation process will create exposed and unexposed regions of the PVA precisely along the predefined folding edges. The subsequent immersion into warm deionized (DI) water (50 °C) will remove the unexposed PVA region and therefore the 2D flake over this part of PVA becomes freestanding, while the exposed PVA region as well as the flake over this region will remain intact. Furthermore, by directing the DI water flow from the unexposed PVA side towards the exposed PVA side, the now free-moving 2D material sheet above the unexposed PVA region will be folded towards the unexposed region to form the folded structure with well-defined position and direction. The spatial control of the folding technique is defined by the EBL process, which is below 100 nm.^[23] A few-layer exfoliated graphene flake before and after folding is demonstrated in **Figure 1b**, which shows a sharp edge after patterning. The folding edge is precisely aligned with the EBL-defined PVA edge, which is critical for accurately controlling the folding direction via changing the

PVA boundary direction. **Figure 1c** shows the scalability of the method for folding 2D material sheet using patterned CVD graphene array. The CVD graphene sample was transferred onto a Si/SiO₂ substrate and patterned into arrays of different length scales before they are further transferred onto PVA/Si substrate using polydimethylsiloxane (PDMS) stamp.^[24] All the patterns were folded in a single process and the yield is 100%. **Figure 1d** shows the atomic force microscopy (AFM) image of a folded graphene flake after removing PVA, demonstrating a clean interface and folding edge.

This fluidic-flow assisted folding also allows the precise control of the folding angle of the resulting structure, utilizing EBL to define the direction of the folding boundary. An angular rotation θ of the folding boundary can result in a 2θ change in the interlayer twist angle, as shown in **Figure 2a**. The smallest twist angle prepared by this technique is about 1°. **Figure 2b** demonstrates the excellent controllability of the folding direction and the resulting twist angles in patterned graphene sheets. By varying the direction of the folding edge, different twist angles such as 30°, 60°, and 90° could be formed in the folded graphene patterns as shown in **Figure 2b**. The accurate control of the folding direction allows the formation of Van der Waals heterostructures with a deterministic inter-layer twist angle. For example, by folding a monolayer graphene into a twisted bilayer with well-defined 12° misorientation angle, a strong G band Raman enhancement can be observed under 532 nm green laser (**Figure 2c**). The enhancement of the G band intensity by more than 30 times results from the Van Hove singularity^[9] caused by a rotational lattice misalignment.^[4,8,10,19,25–28] The twisted angle that can lead to Raman enhancement is proportional to the photon energy of the incident laser (a detailed discussion can be found in Supporting Information). The insignificant D band of the folded

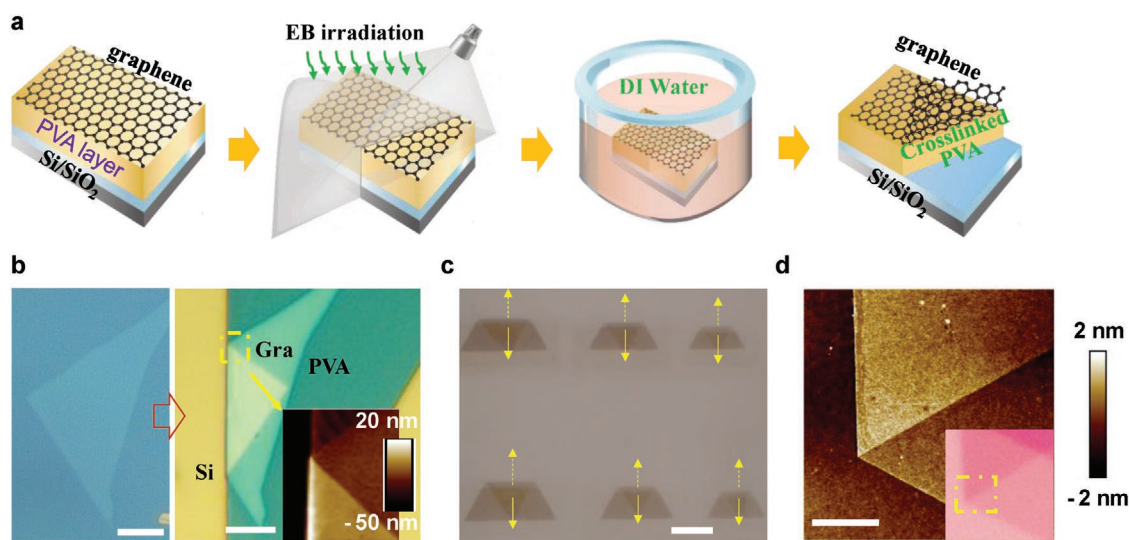


Figure 1. Demonstration of the folding technique. a) A step-by-step illustration of the folding technique; b) A few-layer graphene flake on PVA/SiO₂/Si substrate before and after folding. The AFM image inset shows the folding crease is well aligned with the user-defined PVA edge. c) Deterministic folding of patterned CVD graphene monolayer array under different scales. Dashed and solid arrows indicate the direction of the triangle tip before and after folding, respectively. There is a rectangular PVA layer under each triangular graphene flake, which can be observed by trained eyes. d) An AFM image of a folded graphene sample (after PVA layer is removed) showing the high-quality interface, as well as the well-defined folding edge and folding angle. The inset is the optical microscope image of the same sample, where the area for taking AFM imaging is outlined by a dash line.

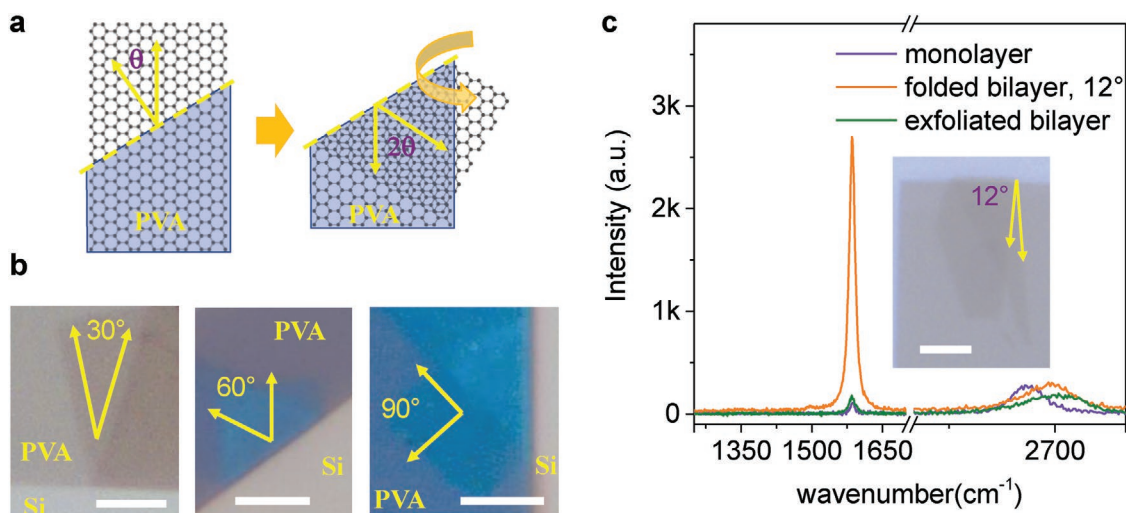


Figure 2. Twisted bilayer graphene with controllable misorientation angle realized by folding for exploring novel physics a) Controlling the folding direction in a graphene sheet by altering the direction of the folding edge. An angular rotation θ between the folding edge, namely the crosslinked PVA edge and the graphene sheet results in a 2θ angular twist between the top and bottom layers in a folded bilayer structure. b) Folded twisted bilayer graphene demonstrates 30° , 60° , and 90° twist angles. In each sample, the PVA layer under the graphene sheet is patterned in a pre-designed direction that leads to the desired twist angle after folding. The folding edge is precisely aligned with the PVA edge, resulting in accurate twist angle control. c) G band Raman enhancement of a twisted bilayer graphene sample prepared by folding a monolayer graphene with a misorientation angle of 12° . The Raman spectrum of an exfoliated mono- and bi-layer graphene flake is also plotted for reference. The wavelength of the incident laser is 532 nm. Scale bar in (b) and (c): $5\ \mu\text{m}$.

bilayer graphene at $\approx 1340\ \text{cm}^{-1}$ suggests the sample is of high quality.

2.2. Molecular Dynamics Simulation and Energy Analysis of the Graphene Folding Process

To understand the fundamental interactions underlying the folding process, we carried out molecular dynamics (MD) simulation to model the folding of a monolayer graphene. A detailed description of the simulation setup can be found in the Supporting Information. **Figure 3** presents configurations and energetics of graphene during folding. Snapshots (a)–(d) show graphene folded at various angles under the flow of water from the unconstrained side. After folding was complete, we turned off the water flow and found that the folding angles remain unchanged.

Figure 3e shows the accumulated work on graphene done by water flow, which reaches equilibrium values of 15 and 23 meV for the two graphene configurations, indicating that graphene sheet with boundary orientation angle $\Phi = 12^\circ$ is slightly harder to fold in water than $\Phi = 0^\circ$. Figure 3f shows the change of the internal energy of graphene with the increase of the folding angle. The energy barrier of folding a single carbon atom is estimated to be around 2 to 3 meV, indicating a small value of the out-of-plane bending modulus of graphene.

Not only does the water fold the graphene, but the graphene affects the water flow. At the onset of graphene folding, we observe an interesting phenomenon in the formation of a wake in the water jet impinging directly on graphene (see movie in the Supporting Information). The wake evolves into a U-shaped pattern as the folding angle increases. The velocity profile in the wake indicates a Levi distribution and the average wake velocity is $300\ \text{m s}^{-1}$.

We also calculate the free-energy difference, ΔF , between folded and unfolded states using Jarzynski's equality^[29]

$$\overline{\exp(-\beta W)} = \exp(-\beta \Delta F) \quad (1)$$

where W represents the work done during folding of graphene. The free-energy difference between folded and unfolded (initial) states of graphene is calculated from MD trajectories in the canonical (NVT) ensemble. The ensemble average in Equation ((1)) involves 20 different initial configurations for each folded state. The free-energy difference per carbon atom increases slowly until the folding angle reaches 90° . Thereafter, the free energy increases more rapidly and reaches a maximum value in the fully folded state. Entropy decrease in graphene sheet is 0.6 and $0.9\ k_B$ for $\varphi = 0^\circ$ and 12° respectively, indicating that 45% to 60% degrees of freedom for free C atoms has been lost after folding.

2.3. Reconfigure the Functionalities of 2D Material Devices through Folding

The experiment and simulation discussed above show that folding of graphene by water flow is feasible. Next, we demonstrate the capability of re-configuring 2D material based devices into various functionalities via our folding technique. Folding can engineer the electrical properties of layered materials by reshaping the Van der Waals sheets' geometry, changing the stack order, and inducing interactions at the interface and folding edges. Such changes can also lead to reconfigurable characteristics at the device level. **Figure 4** shows the re-configuration of a transistor into a floating gate memory device through the folding of 2D material heterostructure involving multiple material layers. As shown in Figure 4a, a heterostructure consisting

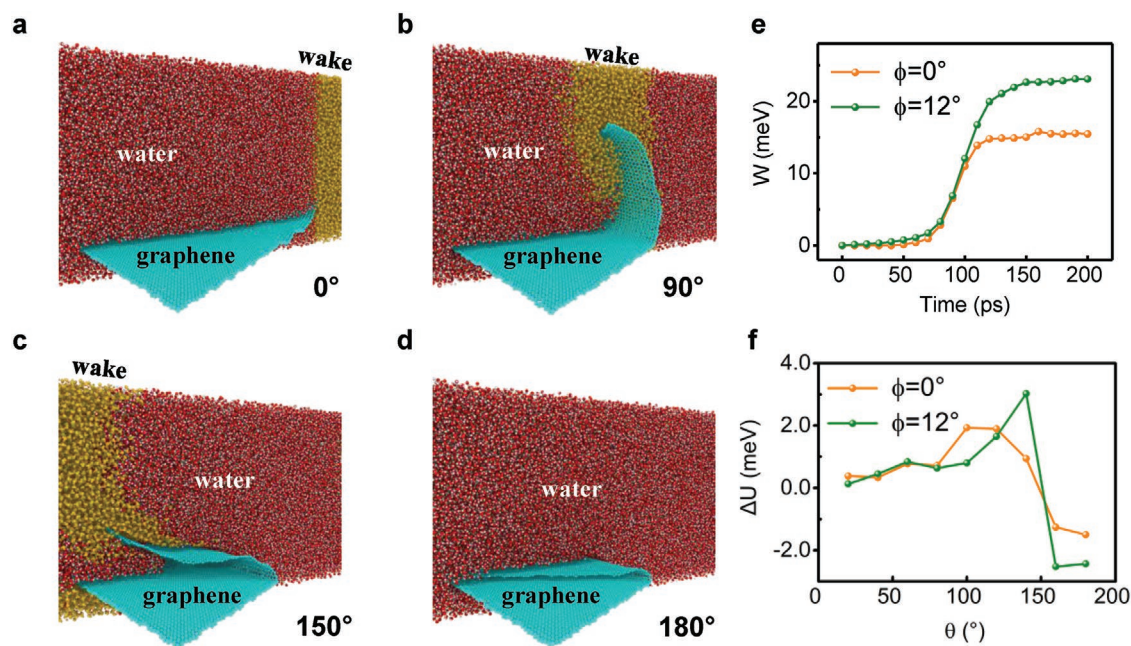


Figure 3. Understanding the folding mechanism by molecular dynamics simulation. a–d) Snapshots show graphene bent under water flow at angles of 0° , 90° , 150° , and 180° , respectively. Here, oxygen and hydrogen atoms in H_2O and carbon atoms in graphene are red, white, and cyan spheres, respectively. Yellow spheres represent molecules in the water wake. Note that only half of the water in the MD box is shown in order to visualize the folding of graphene. e) Per-atom accumulated work done on graphene by water flow as a function of time. ϕ represents the orientation angle of the boundary between fixed and free portions of graphene with respect to the y -axis of the simulation box. f) Changes in the internal energy of graphene as a function of the folding angle θ . The internal energy increases with θ , reaching a maximum value for $\theta = 120^\circ$ and decreases after. The potential energy barrier for graphene folding is around 2 to 3 meV.

of 10 nm hexagonal boron nitride (hBN) sheet, a 10 nm black phosphorus (BP) sheet, and a few-layer graphene sheet was first created, which forms a dual gate transistor structure with BP as the channel material (Figure 4a,b, left panel). The BP transistor exhibits ambipolar conduction behavior where both the electron and hole branches can be reached through electrostatic modulation (Figure 4c), which has been widely reported in previous studies.^[30–33] After folding the heterostructure using the fluidic-flow assisted method along the middle of graphene, the graphene layer becomes embedded inside the BP–hBN stack, serving as a floating gate, where the bottom gate acts as a control gate (Figure 4a,b, right panel).

A positive control gate voltage ($V_{cg,max}$) can shift the threshold voltage of the device positive, and therefore vary the hysteresis windows ΔV_{th} , by increasing the amount of charge stored in the graphene floating gate. Applying a negative control gate voltage, on the other hand, can deplete the stored electrons in the floating gate, which reversibly recovers the V_{th} back to the original value. Hence, by successively sweeping V_{cg} and measuring I_{ds} , we are able to continuously tune V_{th} and obtain different programming states. Figure 4d is a family of $I_{d}-V_{cg}$ curves measured by varying the maximal value of V_{cg} , which shows the memory window, ΔV_{th} is dictated by $V_{cg,max}$, as clearly demonstrated in the inset. To recover a device from positive V_{th} state back to its original state, a negative gate voltage sweep is performed, resulting in a V_{th} almost identical to its original value.

When applying a positive gate voltage, an upward electrical field can cause the tunneling of the electrons in the top BP layer into the graphene floating gate (Figure 4e). The electrons

stored in the graphene floating gate leads to positive shift in the threshold voltage. Similarly, a large negative control gate voltage can remove the electrons from the floating gate through tunneling. Since the BP is n-type under positive gate voltage, we do not consider the minor hole tunneling from the bottom BP layer in this study. The number of electrons stored on the graphene floating gate can be estimated from the expression $n = (\Delta V_{th} \times C_{CG})/q_0$, deduced from charge balance equation,^[34] where q_0 is the elementary electron charge, ΔV_{th} is the threshold voltage shift, C_{CG} is the capacitance between the control gate and the floating gate, which is roughly the capacitance of 90 nm SiO_2 and 40 nm PVA. For each part of the dielectric, the capacitance can be expressed as $\epsilon_0 \epsilon_r / d$, where ϵ_0 is the vacuum permittivity, ϵ_r is the relative dielectric constant of the dielectric (2 for PVA and 3.9 for SiO_2), and d is the dielectric thickness. Given a ΔV of 22 V, the calculated density of electrons tunneling into the floating gate is $\approx 2.8 \times 10^{12} \text{ cm}^{-2}$, a reasonable value considering the relatively thick boron nitride layer (≈ 10 nm). The memory window engineering indicates that the folding process can reconfigure a device with transistor behavior into a device with memory functions.

3. Conclusions

In this work, a fluidic-flow assisted origami technique that can deterministically fold 2D materials and their heterostructures is developed. Using this technique, single-atomic-layer Van der Waals material or their heterostructures with arbitrary

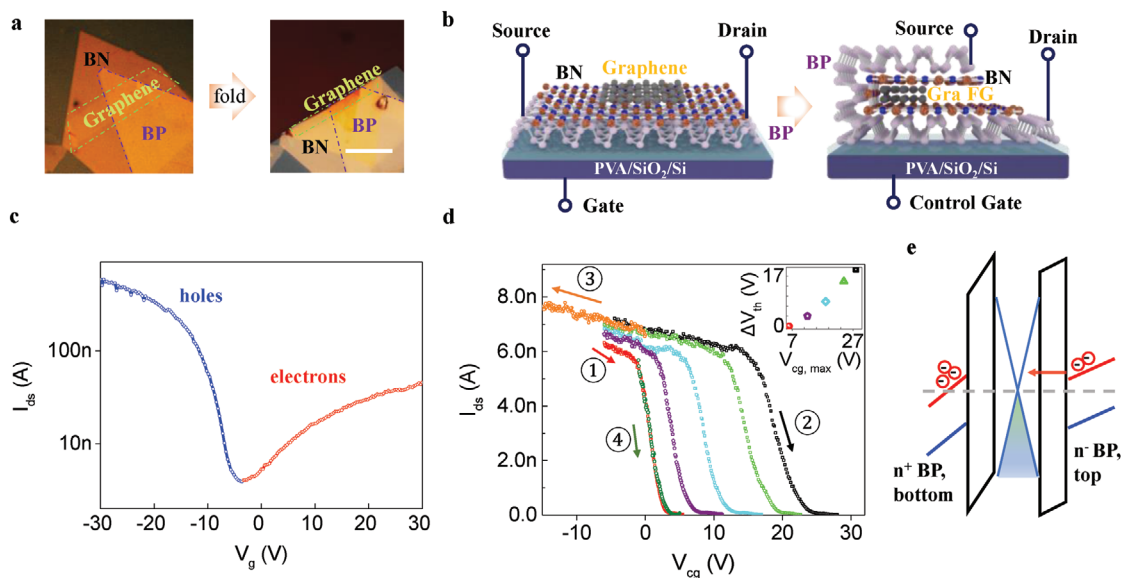


Figure 4. Re-configure a dual gate BP transistor into a floating gate memory device through folding. a) Left: the optical image of the as-fabricated graphene/h-BN/BP heterostructure; right: the image of the sample after folding. Scale bar: 10 μm . b) The sample schematic before and after folding (the schematic is not to scale). The thickness of hBN, BP, and graphene are ≈ 10 , ≈ 10 , and 2 nm, respectively. c) Back gate-dependent current of a typical BP transistor on PVA/Si/SiO₂ substrate before folding shows the ambipolar transistor behavior. The source–drain voltage here is 0.1 V. d) Dependence of the threshold voltage on control-gate voltage V_{cg} , under different V_{cg} maxima were applied before each measurement. I – V transfer characteristics under different programming voltages $V_{\text{cg-max}}$ are plotted. The inset graph shows a linear relationship between the threshold voltage shift versus the maximum programming voltage. Numbers 1 to 4 demonstrate source–drain current measured under different programming state, which shows a complete programming cycle. Red curve: initial state, marked as stage 1; Black curve: transfer curve measured after applying a large control gate voltage (28 V) at the positive direction, which shows V_{th} shift, marked as stage 2; Orange curve: I_{ds} measured with a large negative control gate voltage (–15 V) sweep, which is to erase the state programmed in stage 2, marked as stage 3; green curve: I – V transfer curve is back to the initial state after stage 3, where the V_{th} is almost identical to its original value. e) Band diagram of the folded heterostructure under large positive control gate field. Yellow box and blue cone represent boron nitride and graphene, respectively. The tunnelings of electrons from the top BP layer to graphene floating gate is indicated in the diagram.

scales, thickness, and geometry can be folded without the need of any external supporting polymer layers in the final folded structure. In addition, arrays of patterns can be folded across a large wafer area using this technique and electronic devices that can reconfigure device functions through folding are also demonstrated. The underlying mechanism and energetics of folding are analyzed by molecular dynamics simulations. Such scalable formation of folded Van der Waals material structures with high precision can lead to the creation of new atomic-scale materials and superlattices as well as opening the door to new ways of realizing foldable and reconfigurable electronic devices at micrometer and sub-micrometer scale for memory, sensing, and communication applications.

4. Experimental Section

CVD Graphene Synthesis: Cu foil purchased from Alfa Aesar with 25 μm thickness and 99.8% purity was used as the growth substrate in this work. The growth substrate was subjected to a Ni etchant (Nickel Etchant TFB, Transense) pre-treatment before loading into a low-pressure chemical vapor deposition (LPCVD) system. Similar to previous work,^[35] the growth substrate was then annealed at 1030 °C for 30 min in a hydrogen-rich environment (10 sccm of H₂ at 320 mTorr). In the next 30 min, the LPCVD system was maintained at 1030 °C and 4 sccm of CH₄ was introduced in addition to 10 sccm of H₂, for the graphene synthesis. Finally, the sample cooled down quickly to room

temperature with opened furnace lid. All graphene obtained via this approach was of monolayer thickness.

Deterministic Folding Technique: First, 3 wt% PVA (powder purchased from Sigma-Aldrich) water solution was spin-coated onto Si/SiO₂ substrate, followed with a 2 min baking at 90 °C to form a uniform PVA layer, typically with a thickness of ≈ 40 nm, confirmed by AFM. Then 2D materials were transferred onto PVA/SiO₂/Si substrate with either mechanical exfoliation method^[36] or PDMS stamp based dry transfer technique. Thin samples were identified by optical contrast. The next step was to expose the desired leftover sample area by a standard EBL technique, with a dose of ≈ 5000 $\mu\text{C cm}^{-2}$, to crosslink the PVA. After EBL, the sample was brought in touch with 50 °C DI water. The DI water was purged with high purity nitrogen gas for 20 min to remove oxygen before the sample was submerged in it. The direction of the water flow was aligned with the folding direction to assist the folding. The water flowed over the substrate at a speed of ≈ 10 $\mu\text{m s}^{-1}$. If necessary, the PVA layer underneath 2D material flake could be removed by spincoating a PMMA layer on top of the folded structure and wet transferring the flake onto an arbitrary substrate using KOH solution (1 mol L^{–1}, 90 °C, 2 h) to remove SiO₂,^[37] followed with H₂/Ar (1:3) annealing for 3 h at 350 °C.

Molecular Dynamics Simulation: The initial setup of the MD simulation is shown in Figure S3, Supporting Information. The system consisted of a triangular patch of graphene and 0.27 million water molecules in an MD box of dimensions 24 \times 24 \times 12 nm³. The length of the equilateral triangular graphene sheet was 20 nm. Carbon atoms in graphene interact via the adaptive intermolecular reactive empirical bond order^[38] potential and the transferable intermolecular potential TIP4P/2005^[39] was used for H₂O molecules. The interaction between graphene and H₂O was modeled by Lennard-Jones potential,^[40] whose

parameters were optimized with experimental data on contact angle for H₂O droplets on a graphene substrate.

The hypothesis was that cross-linking of PVA due to irradiation makes the irradiated half of PVA hydrophobic, thereby enhancing the adhesion energy between graphene and irradiated PVA. This enhancement was taken into account by applying a harmonic force to one half of the graphene sample, as shown in Figure S3, Supporting Information. The spring constant of the harmonic force was taken to be 0.16 nN Å⁻¹. If spring extension was taken to be 2 Å, then the corresponding energy is 0.4 J or 16 k_BT. This agrees with experimental estimates of the adhesion energy between graphene and cross-linked PVA. In this simulation the orientation of the boundary between harmonically fixed and free graphene atoms was also considered, the orientation angle was chosen to be $\varphi = 0^\circ$ and 12° , as shown in Figure S2, Supporting Information.

First, an MD simulation was carried out to thermalize the system of graphene immersed in water at 300 K, periodic boundary conditions were applied in every instance and equations of motion, for atoms were integrated with the velocity-Verlet algorithm using a time step of 1 fs. Subsequently, the system was coupled to a heat bath at temperature $T = 300$ K and the unconstrained part of graphene was subjected to water flow (average speed ≈ 200 m s⁻¹) at constant pressure $P = 0.08$ GPa. Another simulation was also carried out at average speed = 100 m s⁻¹ and find the same folding phenomena. It was not expected that the water flow speed affect whether folding occurs; it will only affect the rate of folding.

AFM and Raman Spectroscopy: The AFM image was captured using a Bruker Dimension Icon System under ScanAsyst mode. The Raman spectroscopy was measured with a Renishaw InVia spectrometer with a 532 nm incident laser. A 50 × objective and 100 μW laser power was applied to avoid damaging the samples.

Device Fabrication and Electrical Characterization: The device was patterned by a standard EBL technique after folding, and the metal electrodes were deposited by electron beam metal evaporation. A 2 nm Cr was deposited followed by depositing 50 nm Au. All the devices were measured by a Keysight B1500A parameter analyzer using a lakeshore probe station under $\approx 10^{-6}$ Torr vacuum.

Supporting Information

Supporting Information is available from the Wiley Online Library or from the author.

Acknowledgements

This work is partially supported by the Air Force Office of Scientific Research FATE MURI program (Grant no. FA9550-15-1-0514). J.K. acknowledges the support from the Center for Energy Efficient Electronics Science through NSF (Grant no. 0939514). The simulation work was supported by the Computational Materials Sciences Program funded by the U.S. Department of Energy, Office of Science, Basic Energy Sciences (Grant no. DE-SC0014607). Simulations were performed at the Argonne Leadership Computing Facility under the DOE INCITE program and at the Center for High Performance Computing of the University of Southern California. This work was also performed, in part, at the Center for Integrated Nanotechnologies, an Office of Science User Facility operated for the U.S. Department of Energy Office of Science. Sandia National Laboratories is a multi-mission laboratory managed and operated by National Technology & Engineering Solutions of Sandia, LLC, a wholly owned subsidiary of Honeywell International, Inc., for the U.S. DOE's National Nuclear Security Administration under contract DE-NA-0003525.

Conflict of Interest

The authors declare no conflict of interest.

Author Contributions

H.Z. and H.W. conceived the project idea. H.Z. developed the folding technique, prepared the samples, and fabricated the devices. H.Z. conducted Raman, AFM, device characterizations, and analyzed the data. B.W. performed molecular dynamics simulation with the supervision of P.V., A.N., and R.K. F.L. performed the TEM and EELS characterizations. X.Y. helped with sample preparations. H.Z.W., W.S.L., and J.K. synthesized the CVD graphene samples. M.J.S. contributed analysis of the polymer-graphene interactions. H.W. and R.K. generally supervised the experiment and simulations, respectively. H.Z., B.W., R.K., and H.W. wrote the manuscript with contributions and discussions from other co-authors.

Keywords

2D materials, origami, reconfigurable devices, twisted bilayers

Received: October 21, 2019

Revised: January 7, 2020

Published online: February 14, 2020

- [1] I. Ovid'Ko, *Rev. Adv. Mater. Sci.* **2013**, *34*, 1.
- [2] M. K. Blees, A. W. Barnard, P. A. Rose, S. P. Roberts, K. L. McGill, P. Y. Huang, A. R. Ruyack, J. W. Kevek, B. Kobrin, D. A. Muller, *Nature* **2015**, *524*, 204.
- [3] C. Lee, X. Wei, J. W. Kysar, J. Hone, *Science* **2008**, *321*, 385.
- [4] Y. Cao, V. Fatemi, A. Demir, S. Fang, S. L. Tomarken, J. Y. Luo, J. D. Sanchez-Yamagishi, K. Watanabe, T. Taniguchi, E. Kaxiras, *Nature* **2018**, *556*, 80.
- [5] H. C. Po, L. Zou, A. Vishwanath, T. Senthil, *Phys. Rev. X* **2018**, *8*, 031089.
- [6] J. Yin, H. Wang, H. Peng, Z. Tan, L. Liao, L. Lin, X. Sun, A. L. Koh, Y. Chen, H. Peng, Z. Liu, *Nat. Commun.* **2016**, *7*, 10699.
- [7] I. Brihuega, P. Mallet, H. González-Herrero, G. T. de Laissardière, M. Ugeda, L. Magaud, J. Gómez-Rodríguez, F. Ynduráin, J.-Y. Veuillen, *Phys. Rev. Lett.* **2012**, *109*, 196802.
- [8] R. W. Havener, Y. Liang, L. Brown, L. Yang, J. Park, *Nano Lett.* **2014**, *14*, 3353.
- [9] G. Li, A. Luican, J. L. Dos Santos, A. C. Neto, A. Reina, J. Kong, E. Andrei, *Nat. Phys.* **2010**, *6*, 109.
- [10] Y. Cao, V. Fatemi, S. Fang, K. Watanabe, T. Taniguchi, E. Kaxiras, P. Jarillo-Herrero, *Nature* **2018**, *556*, 43.
- [11] J. Gonzalez, T. Stauber, *Phys. Rev. Lett.* **2019**, *122*, 026801.
- [12] M. Yankowitz, S. Chen, H. Polshyn, Y. Zhang, K. Watanabe, T. Taniguchi, D. Graf, A. F. Young, C. R. Dean, *Science* **2019**, *363*, eaav1910.
- [13] S. Carr, D. Massatt, S. Fang, P. Cazeaux, M. Luskin, E. Kaxiras, *Phys. Rev. B* **2017**, *95*, 075420.
- [14] J. T. Robinson, S. W. Schmucker, C. B. Diaconescu, J. P. Long, J. C. Culbertson, T. Ohta, A. L. Friedman, T. E. Beechem, *ACS Nano* **2013**, *7*, 637.
- [15] C.-J. Kim, A. Sánchez-Castillo, Z. Ziegler, Y. Ogawa, C. Noguez, J. Park, *Nat. Nanotechnol.* **2016**, *11*, 520.
- [16] V. L. Nguyen, D. J. Perello, S. Lee, C. T. Nai, B. G. Shin, J. G. Kim, H. Y. Park, H. Y. Jeong, J. Zhao, Q. A. Vu, *Adv. Mater.* **2016**, *28*, 8177.
- [17] K. Kim, S. Coh, L. Z. Tan, W. Regan, J. M. Yuk, E. Chatterjee, M. F. Crommie, M. L. Cohen, S. G. Louie, A. Zettl, *Phys. Rev. Lett.* **2012**, *108*, 246103.
- [18] P. Y. Huang, C. S. Ruiz-Vargas, A. M. van der Zande, W. S. Whitney, M. P. Levendorf, J. W. Kevek, S. Garg, J. S. Alden, C. J. Hustedt, Y. Zhu, J. Park, P. L. McEuen, D. A. Muller, *Nature* **2011**, *469*, 389.

- [19] R. W. Havener, H. Zhuang, L. Brown, R. G. Hennig, J. Park, *Nano Lett.* **2012**, *12*, 3162.
- [20] C. Schildknecht, *J. Polym. Sci., Polym. Lett. Ed.* **1974**, *12*, 105.
- [21] C.-M. Chuang, M.-C. Wu, Y.-C. Huang, K.-C. Cheng, C.-F. Lin, Y.-F. Chen, W.-F. Su, *Nanotechnology* **2006**, *17*, 4399.
- [22] J. Marqués-Hueso, R. Abargues, J. Canet-Ferrer, S. d. Agouram, J. L. Valdés, J. P. Martínez-Pastor, *Langmuir* **2010**, *26*, 2825.
- [23] R. Abargues, J. Marqués-Hueso, J. Canet-Ferrer, E. Pedrueza, J. Valdés, E. Jiménez, J. Martínez-Pastor, *Nanotechnology* **2008**, *19*, 355308.
- [24] A. Castellanos-Gomez, M. Buscema, R. Molenaar, V. Singh, L. Janssen, H. S. Van Der Zant, G. A. Steele, *2D Mater.* **2014**, *1*, 011002.
- [25] V. Carozo, C. M. Almeida, E. H. Ferreira, L. G. Cancado, C. A. Achete, A. Jorio, *Nano Lett.* **2011**, *11*, 4527.
- [26] A. Jorio, L. G. Cançado, *Solid State Commun.* **2013**, *175-176*, 3.
- [27] Y. Kim, P. Herlinger, P. Moon, M. Koshino, T. Taniguchi, K. Watanabe, J. H. Smet, *Nano Lett.* **2016**, *16*, 5053.
- [28] P. Moon, M. Koshino, *Phys. Rev. B* **2013**, *87*, 205404.
- [29] C. Jarzynski, *Phys. Rev. Lett.* **1997**, *78*, 2690.
- [30] Y. Du, H. Liu, Y. Deng, P. D. Ye, *ACS Nano* **2014**, *8*, 10035.
- [31] H. Wang, X. Wang, F. Xia, L. Wang, H. Jiang, Q. Xia, M. L. Chin, M. Dubey, S.-J. Han, *Nano Lett.* **2014**, *14*, 6424.
- [32] W. Zhu, M. N. Yogeesh, S. Yang, S. H. Aldave, J.-S. Kim, S. Sonde, L. Tao, N. Lu, D. Akinwande, *Nano Lett.* **2015**, *15*, 1883.
- [33] H. Liu, Y. Du, Y. Deng, D. Y. Peide, *Chem. Soc. Rev.* **2015**, *44*, 2732.
- [34] P. Pavan, L. Larcher, A. Marmioli, *Floating Gate Devices: Operation and Compact Modeling*, Springer Science & Business Media, Berlin **2007**.
- [35] H. Wang, W. S. Leong, F. Hu, L. Ju, C. Su, Y. Guo, J. Li, M. Li, A. Hu, J. Kong, *ACS Nano* **2018**, *12*, 2395.
- [36] K. S. Novoselov, A. K. Geim, S. V. Morozov, D. Jiang, Y. Zhang, S. V. Dubonos, I. V. Grigorieva, A. A. Firsov, *Science* **2004**, *306*, 666.
- [37] A. Reina, H. Son, L. Jiao, B. Fan, M. S. Dresselhaus, Z. Liu, J. Kong, *J. Phys. Chem. C* **2008**, *112*, 17741.
- [38] S. J. Stuart, A. B. Tutein, J. A. Harrison, *J. Chem. Phys.* **2000**, *112*, 6472.
- [39] J. L. Abascal, C. Vega, *J. Chem. Phys.* **2005**, *123*, 234505.
- [40] M. Ma, G. Tocci, A. Michaelides, G. Aeppli, *Nat. Mater.* **2016**, *15*, 66.